Theor Appl Climatol (2014) 116:155–168
DOI 10.1007/s00704-013-0934-9

ORIGINAL PAPER

Annual maximum 5-day rainfall total and maximum number of consecutive dry days over Central America and the Caribbean in the late twenty-first century projected by an atmospheric general circulation model with three different horizontal resolutions

T. Nakaegawa · A. Kitoh · H. Murakami · S. Kusunoki

Received: 29 January 2013 / Accepted: 20 May 2013 / Published online: 11 June 2013

Abstract We simulated changes in annual maximum 5-day rainfall (RX5D) and annual maximum number of consecutive dry days (CDD) in Central America, Mexico, and the Caribbean with three different horizontal resolution atmospheric global general circulation models (AGCMs) and quantified the uncertainty of the projections. The RX5Ds and CDDs were projected to increase in most areas in response to global warming. However, consistent changes were confined to small areas: for RX5D, both coastal zones of northern Mexico and the Yucatan Peninsula; for CDD, the Pacific coastal zone of Mexico, the Yucatan Peninsula, and Guatemala. All three AGCMs projected that RX5Ds and CDDs averaged over only the land area and over the entire area (land and ocean) would increase. The dependence of RX5D probability density functions on the horizontal resolutions was complex. Precipitation unrelated to tropical cyclones was primarily responsible for the projected increases in the frequency of RX5Ds greater than 300 mm.

1 Introduction

The region consisting of Central America, Mexico, and the Caribbean has been called a climate change "hot spot" because it is the most responsive of the tropical regions to changes in global climate. Average precipitation and precipitation variability in the region are particularly sensitive to global climate (Giorgi 2006). Previous multi-model ensemble (MME) studies have projected drier summers in the region (Neelin et al. 2006; Rauscher et al. 2008; Campbell et al. 2011). In general, wet-season precipitation is projected to decrease throughout most of the region, and dry-season precipitation is projected to decrease in the areas where orographic precipitation dominates (Karmalkar et al. 2011). Projected changes in the spatial distribution of precipitation are expected to intensify the gradient between the wet northern and dry southern Caribbean during the period from November to January (Campbell et al. 2011). The MME of the Coupled Model Intercomparison Project 3rd phase (CMIP3) also projects a 9 % decrease in annual mean precipitation and more frequent dry extremes in all seasons throughout most of the region by the end of this century under the A1B scenario.

Models with a high horizontal resolution are essential for reliable projections of climate extremes because such resolution is required to simulate the small-scale physical processes that produce and maintain the extremes. In addition, there have been few projections of climate extremes for Central America, especially over the subcontinent itself, because the land areas are not large enough to represent with the horizontal resolutions (about 150- to 300-km mesh, for example) of the CMIP3 and CMIP5 models. Reliable projections of extreme climates over the subcontinent require high-horizontal-resolution atmospheric general circulation models (AGCMs; Kamiguchi et al. 2006; Uchiyama et al. 2006; (Hall et al. 2012) or regional climate models (RCMs) (Campbell et al. 2011; Karmalkar et al. 2008). Most previous studies have suggested increases in heavy

T. Nakaegawa (✉) · A. Kitoh · S. Kusunoki
Meteorological Research Institute, 1-1 Nagamine,
Tsukuba, Ibaraki 305-0052, Japan
e-mail: tnakaega@mri-jma.go.jp

H. Murakami
International Pacific Research Center, University of Hawaii,
Honolulu, HI, USA

precipitation (e.g., Kamiguchi et al. 2006) and hot weather (e.g., Uchiyama et al. 2006). The same changes in extremes are also projected in the Caribbean (Campbell et al. 2011; (Hall et al. 2012) and in Costa Rica (Karmalkar et al. 2008). An Intergovernmental Panel on Climate Change (IPCC) special report on extreme events (SREX; Senevirante et al. 2012) mentions no publications related to extreme climates in Central America and the Caribbean except for those cited above.

Because uncertainties in the structures of models have nontrivial effects on future climate projections (Christensen et al. 2007), ensemble experiments with multiple high-horizontal-resolution RCMs forced with multiple lower and lateral boundary conditions have been performed in countries with advanced computational facilities (e.g., Christensen et al. 2007; van der Linden and Mitchell 2009; Arritt and Rummukainen 2011), but such simulations require advanced modeling technologies and huge computational resources. For Central America and the Caribbean, previous high-horizontal-resolution AGCM and RCM approaches have typically used a single projected lower boundary condition and lateral boundary condition obtained from CMIP3 models. The result obtained with such approaches is a sample projection, but with no quantified uncertainty related to the structure of the model. To quantify the uncertainties in climatological mean changes, Christensen et al. (2007) used the consistency of a change in sign among the MME in IPCC fourth assessment report (AR4).

Another difficulty in projecting extreme climates is the high sensitivity to the horizontal resolution of the models. As mentioned above, high-horizontal-resolution models are prerequisite for projections in Central America and the Caribbean. There is a decrease in the 30-year return levels of daily precipitation and simple daily intensity index when they are estimated with lower horizontal resolution models in the continental United States (Cheng and Knutson 2008). The difference results from the resolution dependency of the amounts of extreme precipitation and the difficulty in quantitatively assessing changes in extreme precipitation at local scales in South America (Kitoh et al. 2011). It is unclear to what extent these results apply to Central America and the Caribbean.

In the present study, we used a high-horizontal-resolution AGCM with an ensemble approach to explore potential future changes in precipitation-related extremes and their uncertainties in Central America and the Caribbean. In addition, we examined the dependency of simulated future changes of extreme climate events on the horizontal resolution of the AGCM. We used two annual precipitation-related extreme indices: the annual maximum 5-day rainfall total (RX5D) as a heavy precipitation index and the annual maximum number of consecutive dry days (CDD) as a dryness index (e.g., Frich et al. 2002).

2 Methodology

2.1 Model and experiments

The Meteorological Research Institute (MRI) and the Japan Meteorological Agency developed a global hydrostatic AGCM (MRI-AGCM3.1; Mizuta et al. 2006). We conducted 25-year integrations with the MRI-AGCM3.1 for the present-day climate (1979–2003) and a future climate (2075–2099) at three different horizontal resolutions: the T_L959 (a grid size of 20 km; 3.1S), T_L319 (60 km; 3.1H), and T_L95 (180 km; 3.1 L) (Kitoh A, Ose T, Kurihara K, Kusunoki S, Sugi M, KAKUSHIN Team-3 Modeling Group 2009). As lower boundary conditions, observed monthly sea surface temperatures (SSTs) and sea-ice concentrations (HadISST; Rayner et al. 2003) were prescribed for the present-day climate simulation; a dataset of the monthly SST data and sea-ice concentrations averaged by the 18 CMIP3 GCM projections under the SRES A1B (Mizuta et al. 2008) were prescribed as lower boundary conditions for the future climate simulation. This type of future climate simulation is called a time-slice experiment and was first used by Bengtsson et al. (1996) to project the characteristics of tropical cyclones in a future climate scenario. Such an experiment may include some disadvantages, such as the temporal variabilities that remain in present-day climate simulations; however, such simulations are widely used for climate projections (e.g. Kamiguchi et al. 2006; Kitoh et al. 2011; Jung et al. 2012). This experiment is the same simulation used by Hall et al. (2012)), who projected the future climate in the Caribbean.

We used 60- and 180-km mesh models to conduct ensemble experiments with three other lower boundary conditions to quantify the uncertainty in climate change projections. The other three different lower boundary conditions were the CSIRO-Mk3.0, MRI-CGCM2.3.2, and MIROC3.2(hres) SSTs (see Table 1 in Kitoh et al. (2011) for details). The MIROC3.2(hres) SSTs show a La Niña-like spatial feature in the tropical Pacific, whereas the other three SSTs as well as the CMIP3 MME SST show an El Niño-like pattern. Each SST experiment consisted of three-member simulations with different initial conditions, and the ensemble experiment therefore comprising a 12-member (4 lower boundary conditions×3 initial conditions) ensemble for the projection of future climate.

2.2 Two precipitation-related extreme indices

As mentioned in Section 1, the RX5D and CDD have been widely used as precipitation-related indices in SREX (Senevirante et al. 2012) and previous studies (e.g., Kamiguchi et al. 2006; Kitoh et al. 2011; Hall et al. 2012). In addition to the RX5D and CDD, we used three other indices in our analysis. One was the annual maximum 5-day

rainfall due to precipitation associated with tropical cyclones (TCs), where TC-induced precipitation was defined as precipitation within 500 km of the center of the TC. Many different algorithms have been used to identify TCs (e.g., Vitart and Stockdale 2001; Walsh et al. 2007; Takaya et al. 2010). The TC detection algorithm we used includes the following five globally uniform criteria of Murakami and Sugi (2010): relative vorticity at 850 hPa, temperature anomaly in the warm-core region, maximum wind velocity at 850 hPa, genesis location, and duration. The resolution-dependent value of the relative vorticity at 850 hPa is calibrated to ensure that the annual number of TCs globally in the present-day climate simulation equals the number in the observation data set (84.8 TCs per year for the period 1979–2003). The two other indices were the mean lengths of dry and wet spells, dry and wet days being defined as days when the precipitation was less than or greater than 1 mm, respectively.

2.3 Quantification of uncertainty

In the present study, two metrics were used to quantify uncertainties in projected future changes in climate. One metric was the consistency of a change in sign, a metric that is commonly used in the IPCC AR4 mentioned above as well as in previous studies (e.g., Kitoh et al. 2011). The result for the 60-km mesh model ensemble is the ensemble mean of the 12 members characterized by four different lower boundary conditions and three initial conditions. Because the initial conditions have little effect on the climatologies for a given lower boundary condition, we estimated the two extreme indices from a 75-year (25 years × 3 initial conditions) simulation for each lower boundary condition. We then counted the number of consistent changes in sign of the extreme indices among the four SST future climate ensembles. We considered a projected change to be consistent if there were four same changes in sign.

The other metric was the ratio of the mean of the four SST ensemble changes to the standard deviations of the changes among each of the 75-year experimental SST simulations. That ratio represents the so-called signal-to-noise ratio, where the signal is the mean of the four SST ensemble changes, and the noise is the standard deviation (i.e., uncertainty) of the changes among the four SST ensemble experiments. The ratios indicate how large the changes are compared to the uncertainties. Larger absolute values of the ratio imply a higher signal-to-noise ratio in the projected changes.

2.4 Observational data

To verify the simulated geographic distribution of the RX5D and CDD, we used the One-Degree Daily dataset of the Global Precipitation Climatology Project (GPCP1DD; Huffman et al. 2001) and the 0.25° 3-hourly Tropical Rainfall Measuring Mission (TRMM) 3B42 V6 dataset (Adler et al. 2000). A dry day was defined to be a day with less than 1 mm of precipitation (e.g., Frich et al. 2002). The periods of time associated with the two datasets were not exactly consistent with the present-day (1979–2003) climate simulation. The GPCP1DD includes 14 years from 1997 to 2010, and the TRMM 3B42 includes 13 years from 1998 to 2010. However, the two datasets allow qualitative comparisons with the indices in the model simulations.

2.5 Study area

The study area extended from 8°N to 32°N and from 58°W to 115°W, the focus being only on Mexico, the subcontinent of Central America, and the islands of the Caribbean. The horizontal resolution of the models affected the details of representations of topographic features and land–sea distributions (Fig. 1). The 20-km-mesh model captured the four Sierra Madre ranges in Mexico and Guatemala and the Greater Antilles well but not and the Lesser Antilles, whereas the 60-km-mesh model failed to capture these details, especially the Lesser Antilles. In the 180-km-mesh model, the Isthmus of Panama was not contiguous, and the mountain peaks in the area were reduced in height.

3 Reproducibility

As a fundamental prerequisite, the climatological annual mean precipitation must be well simulated in models of future climates. Of the three different horizontal resolution MRI-AGCMs, the 20-km-mesh model provided the best simulation of the amount and spatial distribution of the climatological annual mean precipitation (Fig. 2). Detailed features of the geographical distributions such as the Intertropical Convergence Zone and meridional gradients of climatological annual mean precipitation were simulated better by the 20-km-mesh model than by the 60-km-mesh and 180-km-mesh models. The 20-km-mesh model also simulated distinct orographic precipitation, although such precipitation is not found in the TRMM 3B42 dataset. The three models overestimated the climatological annual mean precipitation. The 20-km-mesh model simulated the climatological seasonal mean precipitation in the Caribbean (Hall et al. 2012) and globally (Mizuta et al. 2006; Kitoh A, Ose T, Kurihara K, Kusunoki S, Sugi M, KAKUSHIN Team-3 Modeling Group 2009) as well as the climatological annual mean precipitation. Such advantages of a high-horizontal-resolution model in the study area were also demonstrated by comparisons between a 25-km-mesh regional climate model and 300- to 400-km-mesh GCMs (Karmalkar et al. 2011).

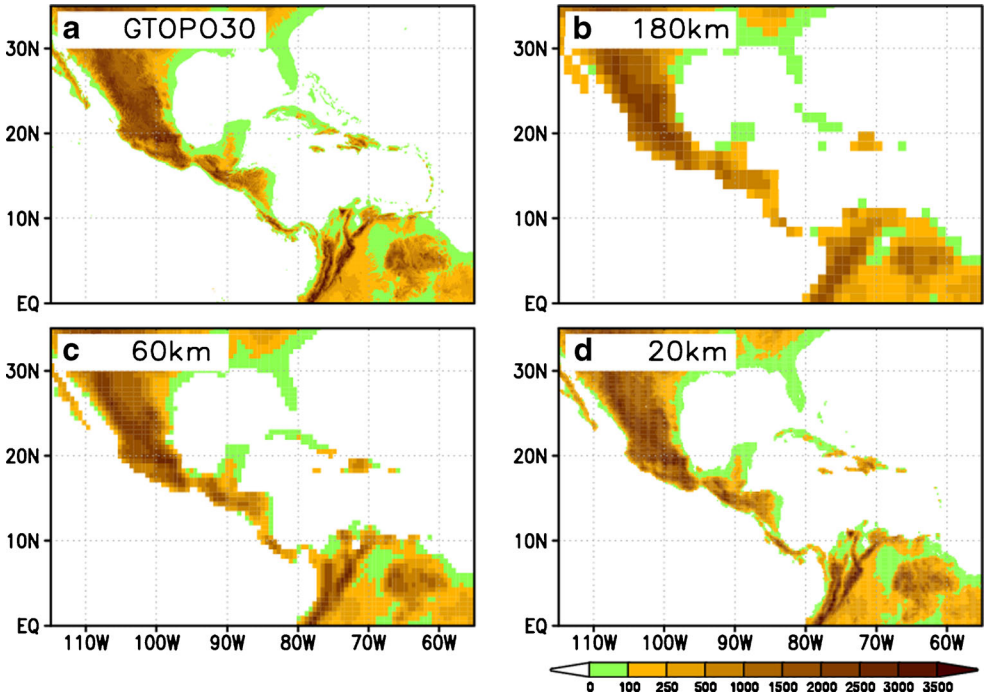

Fig. 1 Study area and grids for **a** GTOPO30 observational data and **b** 180-km-mesh, **c** 60-km-mesh, and **d** 20-km-mesh models. Elevations are in meters

GPCP1DD and TRMM 3B42 observations show the consistent spatial pattern of RX5D, but differences in magnitude because of differences in their data periods and horizontal resolutions (Fig. 3a, b; Table 1). Large values of RX5D are scattered throughout Central America and the Caribbean in both observational datasets. Of the three different horizontal resolution models, the 20-km-mesh model (Fig. 3e), best represents the spatial pattern of RX5Ds in both sets of observations (Table 2). The root mean square difference between observed and modeled RX5Ds is smallest for the 60-km-mesh model (Fig. 3d) in the case of GPCP1DD and smallest for the 20-km-mesh model in the case of TRMM. The discrepancies in RX5Ds between the two sets of observations are similar to or slightly less than the discrepancies between the three different horizontal resolution models (Table 2). The 20-km-mesh model reproduced the large-scale pattern and intensity of RX5Ds well, but with slight underestimation of intensity on the Atlantic side. Both the 60-km- and 180-km-mesh models

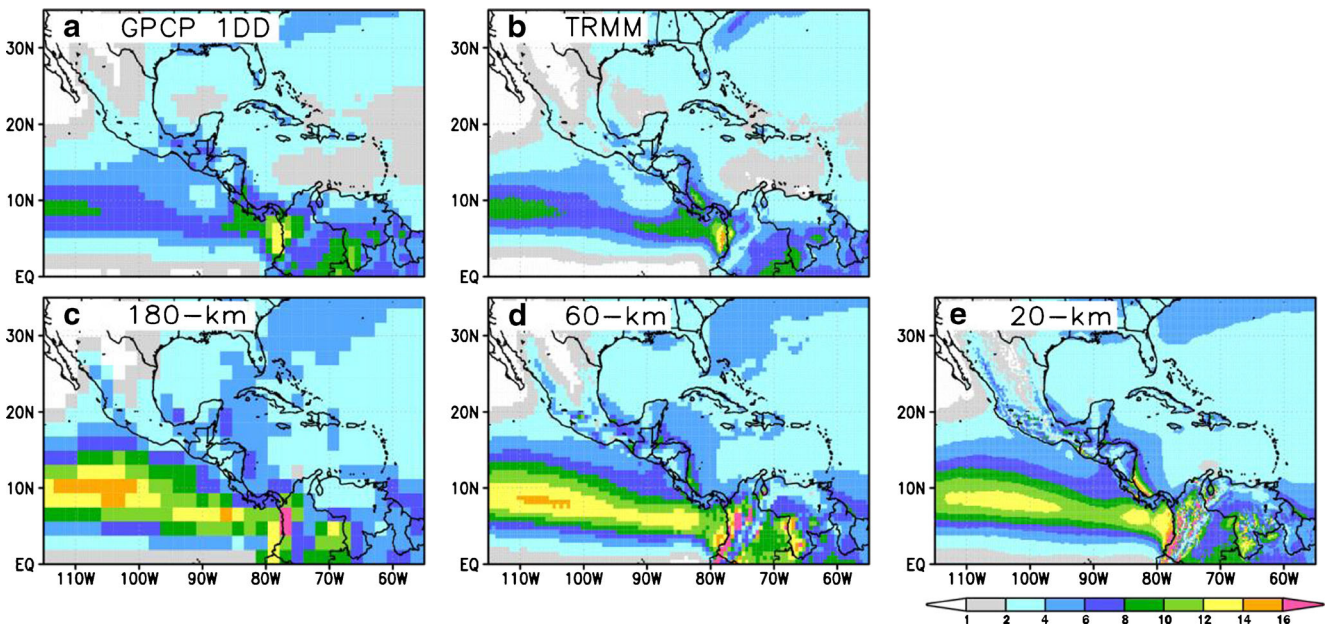

Fig. 2 Geographic distribution of annual mean precipitation (millimeters per day), in observational datasets **a** GPCP1DD and **b** TRMM 3B42, and in the **c** 180-km-mesh, **d** 60-km-mesh, and **e** 20-km-mesh models

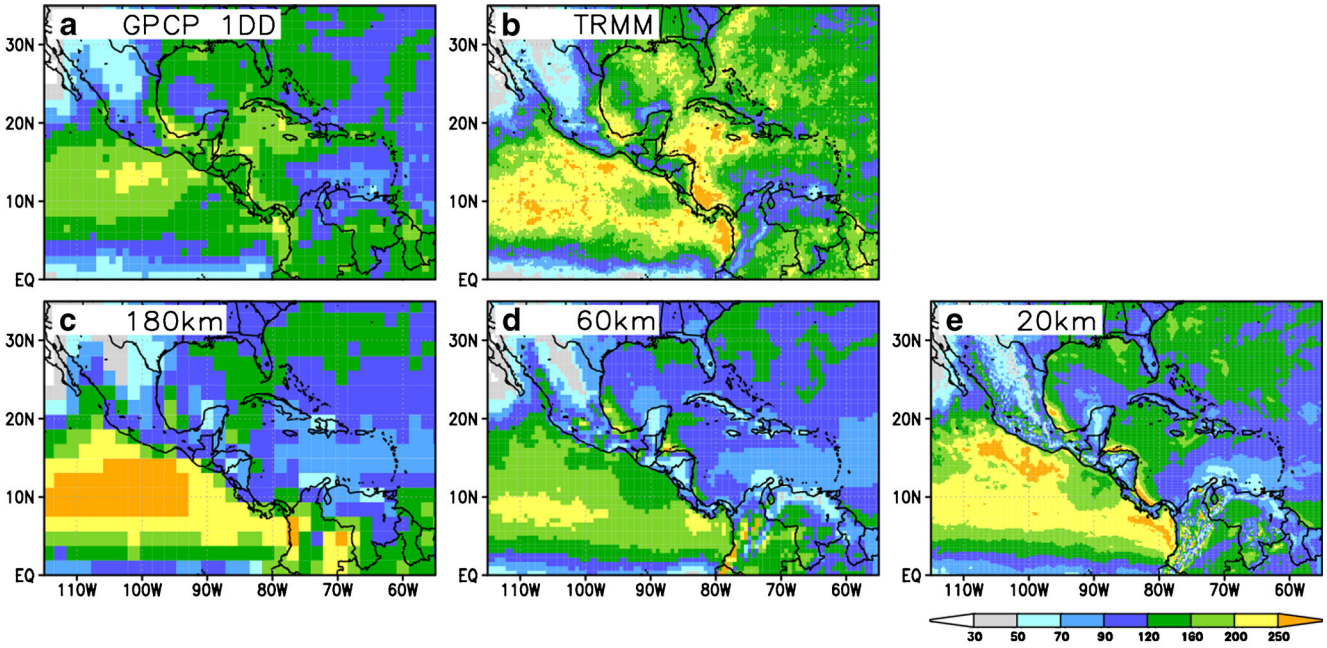

Fig. 3 Geographic distribution of annual maximum 5-day rainfall total (RX5D), in millimeters, in observational data sets **a** GPCP1DD and **b** TRMM 3B42, and in the **c** 180-km-mesh, **d** 60-km-mesh, and **e** 20-km-mesh models

failed to reproduce the intensity of RX5Ds on the Caribbean Sea. The 20-km-mesh model accurately simulated the climatological mean annual orographic precipitation over most land areas in the domain, and so the 20-km-mesh model accurately reproduced RX5Ds in the Sierra Madre ranges and along the Caribbean coast from Nicaragua to Panama. However, all three models reproduced the spatial pattern of RX5Ds fairly well around the Yucatan Peninsula.

The CDDs were shorter in the GPCP1DD than in the TRMM 3B42 (Table 1), although their large-scale spatial patterns were similar (Fig. 4a, b). The spatial patterns of CDDs were very similar in the three models (Table 2); however, the CDD values were shorter in the high-resolution model than in the lower resolution models (Fig. 4c–e; see also Table 1), especially in central and northern Mexico and the northern Caribbean, e.g., Cuba and the Hispaniola Islands (Hall et al. 2012). A possible reason may be the use of the Arakawa-Schubert scheme for cumulus convection in the MRI-AGCM3.1. It is designed for low-horizontal-resolution models and tends to produce frequent light precipitation and hence reduces CDD values. The 20-km-mesh model reproduced CDDs well both qualitatively and quantitatively (Table 2), except over the Atlantic Ocean, whereas the 180-km-mesh model failed to capture the small-scale spatial features of the CDD distribution. The differences in CDDs between the two sets of observations are larger than the analogous differences between the TRMM and the 20-km-mesh model (Table 2).

Campbell et al. (2011) compared the linear trends in observed RX5Ds and CDDs with the RX5Ds and CDDs simulated with the regional climate model in the Caribbean and found few similarities. These results are consistent with the small number of significant linear trends with the Pearson product–moment correlation coefficient at the 95 % confidence level in our simulations (not shown), the

Table 1 RX5D and CDD averaged in the study area for the present-day and future climates and for the three different horizontal resolution models

		Observation		AGCM					
		GPCP	TRMM	180-km		60-km		20-km	
		1DD	3B42	Present	Future	Present	Future	Present	Future
RX5D (mm)	Land	110.1	113.6	88.0	103.6	80.5	85.1	95.3	102.0
	Land+ocean	125.8	154.5	129.0	145.4	109.9	114.6	131.2	134.5
CDD (day)	Land	53.1	56.6	44.5	49.7	40.6	44.5	34.7	37.0
	Land+ocean	37.9	38.2	36.2	39.4	34.4	37.8	35.3	38.5

Table 2 Comparison of RX5D and CDD in the present-day climate between observations and models with different horizontal resolutions

		Observation		AGCM		
		GPCP	TRMM	180-km	60-km	20-km
RX5D (mm)	GPCP		37.34	47.77	35.04	38.76
	TRMM	0.87		50.39	52.81	43.17
	180-km	0.66	0.66		37.73	35.99
	60-km	0.62	0.65	0.87		31.38
	20-km	0.67	0.71	0.81	0.86	
CDD (day)	GPCP		27.67	40.04	41.72	33.51
	TRMM	0.81		31.04	31.46	24.81
	180-km	0.71	0.79		12.64	19.73
	60-km	0.69	0.82	0.97		13.97
	20-km	0.71	0.85	0.92	0.97	

For each index, the number in the upper right is the root mean square differences, and the remaining numbers are the spatial correlation coefficients

lack of statistical significance probably reflecting the large natural variability or noise in the data. The reproducibility of these simulations may be reasonable because there is considerable disagreement in the extreme indices calculated from observations (Figs. 3 and 4), and the 20-km-mesh model appears to be the most suitable for projecting future changes given that its simulation of the present-day climate was better than the analogous simulations of the 60-km- and 180-km-mesh models (e.g., Kamiguchi et al. 2006; Kitoh et al. 2011). These results allowed us to project the two precipitation-related indices to the period from 2075 to 2099.

4 Future projections

4.1 Geographical distribution

The projections of both the 20- and 60-km-mesh ensemble models indicated that RX5Ds would increase in the future throughout most of the study area (Fig. 5). Increases of RX5Ds occurred over 76 and 80 % of the study area in the 20- and 60-km-mesh ensemble models, respectively. Previous studies have projected similar patterns (Kamiguchi et al. 2006; Tebaldi et al. 2006; Campbell et al. 2011). The 20-km-mesh model projected larger changes of RX5Ds than the 60-km-

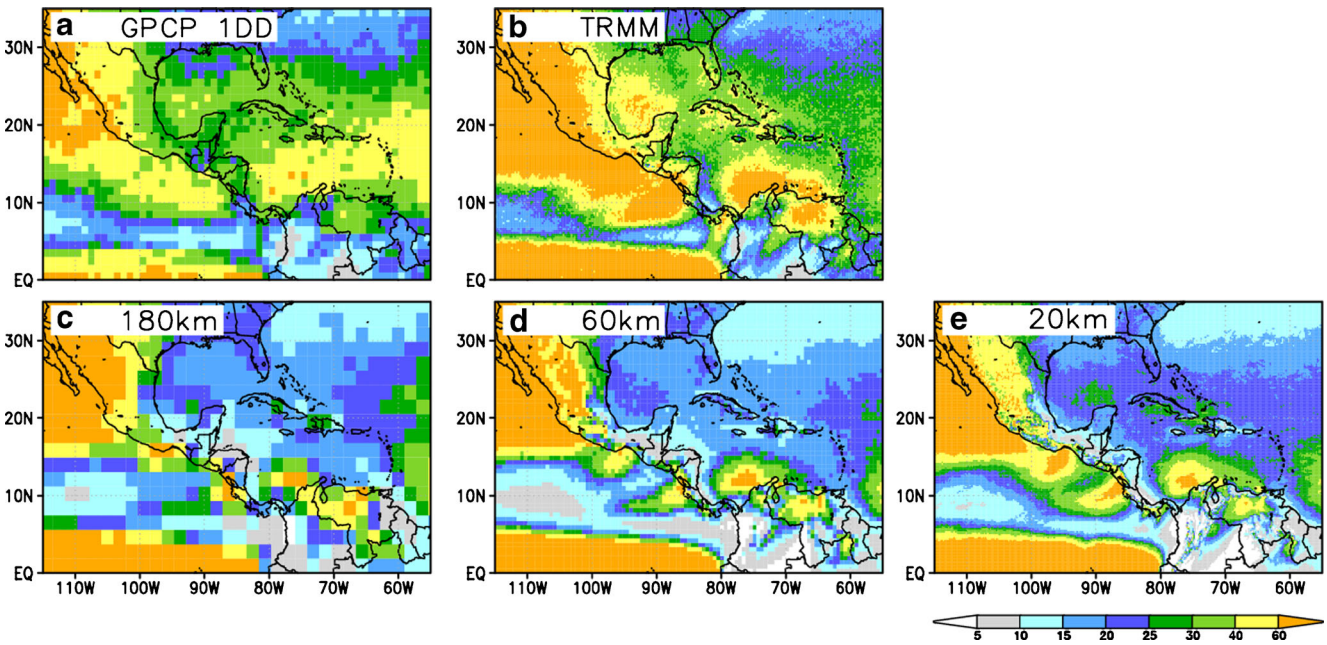

Fig. 4 Same as in Fig. 3 but for the annual maximum number of consecutive dry days (CDD)

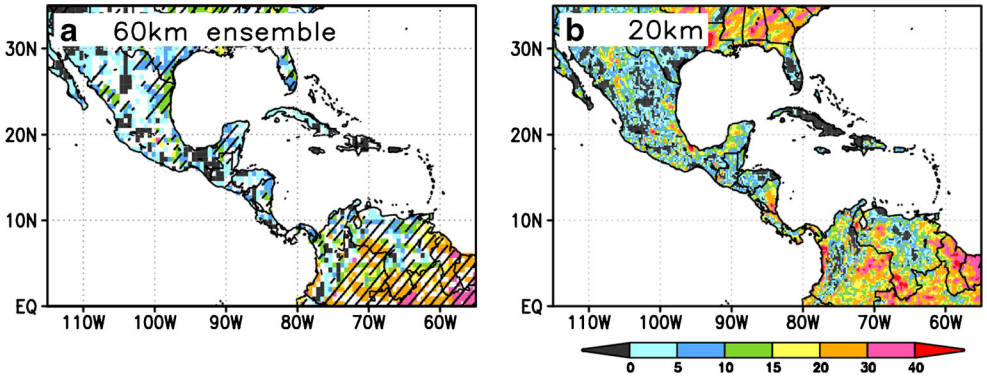

Fig. 5 Changes in RX5D (millimeters) between the present-day and the future for the **a** 60-km-mesh model ensemble and **b** 20-km-mesh model. Areas statistically significant with Weltch's *t* test at the 95 % confidence level are colored. Hatches in (**a**) indicate areas where all four different SST experiments project changes of the same sign

mesh model ensemble; the areal means of changes in RX5Ds were 6.7 mm for the 20-km-mesh model and 5.0 mm for the 60-km-mesh model ensemble. Insignificant changes in the 60-km-mesh model ensemble with Weltch's test at the 95 % confidence level appeared in central Mexico and several small areas such as western Nicaragua. Areas with small changes in RX5D in the 20-km-mesh model were apparent between 10°N and 20°N, especially 12–15°N, an area in the rain shadow of a mountainous area that is represented in the 20-km-mesh model but not in either the 60-km- or the 180-km-mesh model (Fig. 6). The changes were larger along the Pacific Ocean than over Caribbean Sea, and they were positive in the 60-km- and 180-km-mesh models. The analogous changes were opposite in sign in the 20-km-mesh model.

Areas where there were consistent changes in sign were confined to both of the coastal zones of northern Mexico, the Yucatan Peninsula, and some scattered areas (Fig. 5a). There were no such areas on the islands of Cuba and Hispaniola. These islands correspond to areas where there were statistically significant changes in RX5D, but the statistically significant changes in sign were not associated with consistent changes in sign. This result indicates that the statistical significance of a change does not always indicate that there is consistency in the sign of the change, although it generally does so in the case of climatological means (e.g., Kitoh et al. 2011; Nakaegawa et al. 2013a; Fábrega et al. 2013). The absolute values of the signal-to-noise ratios were less than 0.5 in most areas. Absolute values of the signal-to-noise ratio were greater than one in the southern part of the Mexican Plateau, the coastal region around the Gulf of California, and in scattered areas (Fig. 7). The ensemble mean changes were significant in these areas, but the changes in sign were not consistent (Fig. 5a). Such a difference can occur because only the sign of a change determines the consistency of a change in sign, whereas the ratio depends on the variability of the change around the ensemble mean. This fact suggests that uncertainties should be quantified in multiple metrics.

The RX5Ds induced by tropical cyclones were projected to decrease along the Pacific coast of Central America and south of 16°N in the Caribbean Sea, but to increase along the coastline of the Gulf of Mexico and the Yucatan Peninsula (Fig. 8). Murakami and Wang (2010) projected that the frequency of TCs would increase slightly in the North Atlantic Ocean in the future climate, a conclusion that is consistent with the decrease in the magnitude of TC-induced RX5Ds. The 20- and 60-km-mesh model

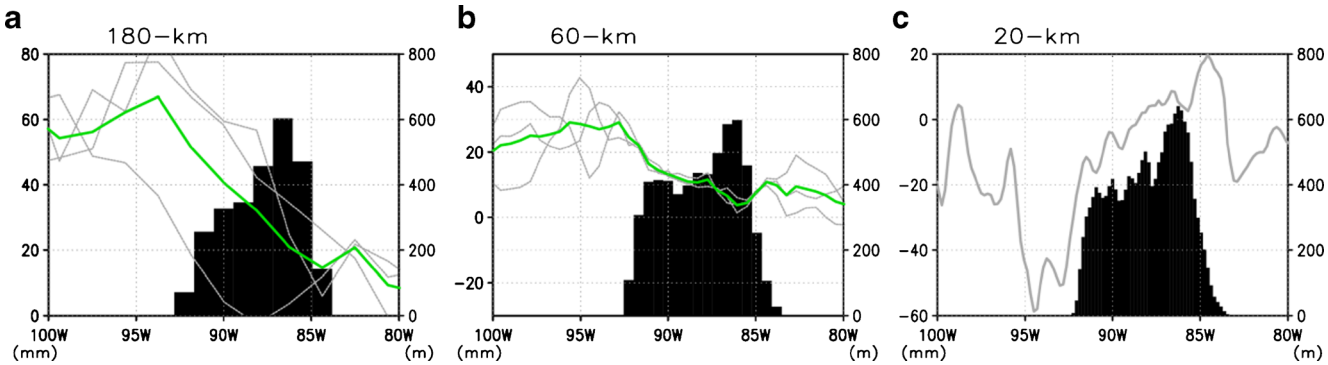

Fig. 6 Vertical cross section showing changes in RX5D (millimetres per day) averaged for 12–15°N between the present-day and the future for **a** 180-km-mesh model, **b** 60-km-mesh model, and **c** 20-km-mesh model. MME mean lower boundary conditions were used in these experiments. *Green lines* represent three-member ensemble means, whereas *gray lines* indicate individual members of the ensemble. Black shading indicates topography of the models

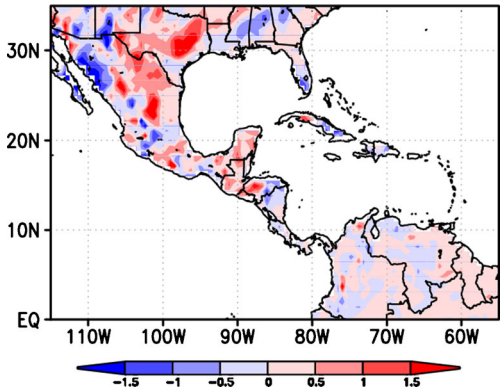

Fig. 7 Ratio of the ensemble mean changes to the standard deviations of the changes for each SST experiment as a metric of the uncertainty of the changes of RX5Ds in the 60-km-mesh ensemble

ensembles both indicated that the areal mean of the RX5Ds in the study area would be greater during the period 2075–2099, as mentioned above. This fact suggests that the projected increase of RX5Ds was due to precipitation events unrelated to TCs rather than to precipitation generated by TCs in the study area.

Increases in precipitation extremes during recent years have been detected on the basis of observations in Central America (Aguilar et al. 2005) and other regions. Min et al. (2011) showed that anthropogenic increases in greenhouse gases have contributed to the observed increase in precipitation extremes over approximately two thirds of Northern Hemisphere land areas. Therefore, the increase of RX5D in Fig. 5 probably stems from anthropogenic increases in greenhouse gases because we used the SRES A1B emission scenario in which human activities play an important role.

The 60-km-mesh model ensemble projected a significant increase of CDDs with Weltch's test at the 95 % confidence level (Fig. 9) in the study area, except for eastern and southern Mexico. The spatial pattern of the CDD changes in the 60-km-mesh model ensemble resembled that of the

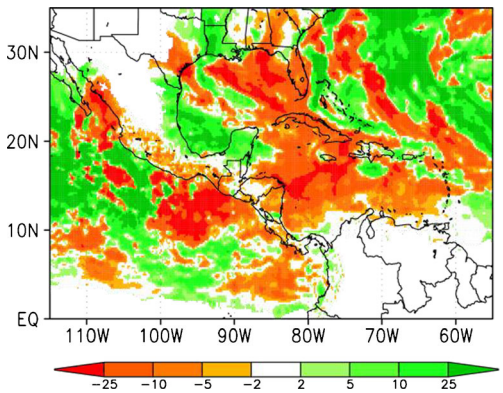

Fig. 8 Changes in TC-induced RX5Ds (millimeters) in the 20-km-mesh model. Colors indicate areas where the frequency of TC occurrence was greater than 0 for both climates

20-km-mesh model. Both models showed large areas in western Mexico within which increases in CDDs were greater than 10 days, whereas only the 60-km-mesh model ensemble projected large increases in Nicaragua and western Panama. Dryness in this domain is partly due to a stronger Caribbean Low Level Jet (CLLJ), which is found in the southwestern Caribbean basin along a zonal axis near 15°N. In the future (2075–2099), the CLLJ is projected to persist through November (Taylor et al. 2012) but not consistent among CMIP3 models (Nakaegawa et al. 2013b). The CLLJ is associated with higher surface pressures, increased vertical wind shear, and reduced moisture convergence and convection (Knaff 1997).

The signs of changes in the CDDs were consistent in most of the study area except for the northern coastal region bordering the Gulf of Mexico, the Greater Antilles, and landmasses south of about 12°N (Fig. 9a). The relationship between the consistency of these changes and their statistical significance was qualitatively similar to the analogous relationship for the RX5Ds. Figure 10 shows the geographical distribution of the ratio of the ensemble mean CDD changes to the standard deviations of the changes for each SST experiment. Absolute values greater than one were confined to the Mexican Plateau, the northern coastal region bordering the Gulf of Mexico, and the northern coastal region surrounding the Gulf of California. These areas are included among the regions where the sign of the changes in CDD was consistent, but a comparison of Figs. 9a and 10 reveals that areas where the sign of the change in CDD was consistent were not necessarily areas where the ratio of the mean to standard deviation was greater than one. There were almost no scattered areas with ratios greater than 0.5 because CDDs are primarily determined by large-scale atmospheric circulation.

Kamiguchi et al. (2006) analyzed future changes in the two extreme indices by using an experimental dataset generated with a previous version of the 20-km-mesh model, MRI-AGCM3.0S, and future SSTs projected by the MRI-CGCM2.3.2 under the SRES A1B scenario. The general features of the projected changes of both indices reported by Kamiguchi et al. (2006) and calculated in the present study resemble each other. Significant changes were limited in areal extent in both studies, and most of the changes were increases of both indices. Marked differences between the results of Kamiguchi et al. (2006) and some results from the present study are apparent in the Greater Antilles: Kamiguchi et al. (2006) and our 20-km-mesh model projected a decrease in RX5Ds, but our 60-km-model ensemble projected an increase.

Simultaneous increases in RX5D and CDD could occur in the future if there are fewer precipitation events but greater amounts of rainfall per event. Tebaldi et al. (2006) used the CMIP3 MME analysis to calculate simulated

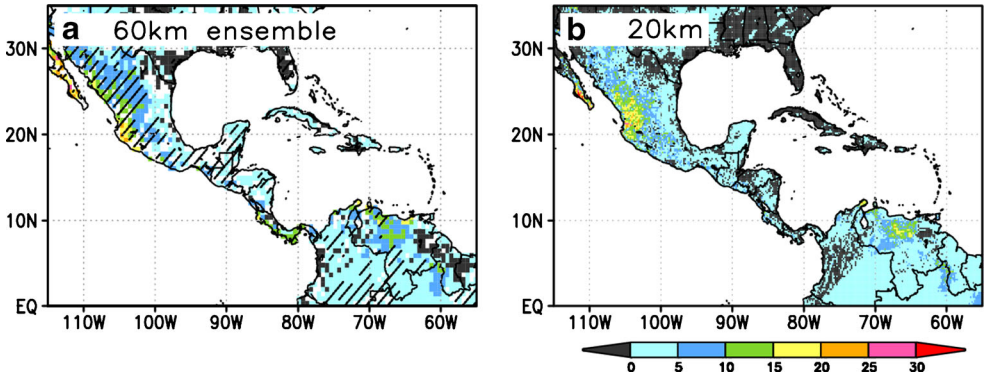

Fig. 9 Same as in Fig. 5, but for CDD (day)

differences in RX5D and CDD between two 20-year periods (2080–2099 minus 1980–1999) for the A1B scenario and evaluated their consistency. Although they found no part of the study area with highly consistent changes in precipitation intensity, we compared our results with theirs because the study by Tebaldi et al. (2006) is one of the few studies that have treated projections of extreme events in Central America and the Caribbean. Tebaldi et al. (2006) projected that RX5Ds would increase on the Caribbean side of the study area and decrease on the Pacific side, whereas the projections of the present study indicate that RX5Ds will significantly increase on both sides, but with high consistency only on the Caribbean side. Both studies show a consistent increase of CDDs throughout the whole study area. In addition, results of both studies are highly consistent in Mexico, except for the eastern part. The similarity of the two projections reinforces the consistency of the results of the present study under SRES A1B.

4.2 Frequencies

In this subsection, we report the results of our analysis of the effects of horizontal resolution on changes in simulated RX5Ds and CDDs. Note that in this analysis we used the three-member simulations of the 60-km- and 180-km-mesh models forced only with the lower boundary conditions obtained from CMIP3 MME means to make it possible to compare those results with the simulated results from the 20-km-mesh model with the same forcing conditions.

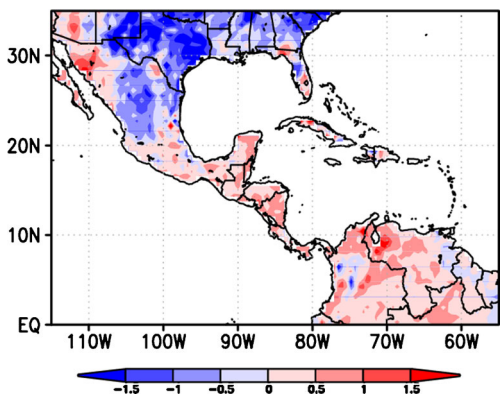

Fig. 10 Same as in Fig. 7 but for CDD (day)

4.2.1 RX5D

The areal mean RX5D was projected to increase in the future for all three horizontal resolutions, but with very low statistical significance or insignificance with Weltch's test at 95 % confidence level (see Table 1). This low significance reflects the fact that the study area covers a variety of climatological mean RX5Ds. As seen in Fig. 5a, there are many grids with significant changes. Under these circumstances, the RX5D probability density functions (PDFs) provide more information than the areal mean RX5D.

Figure 11 depicts the RX5D PDFs for the three different horizontal resolutions. The peak of the PDF near 60 mm was

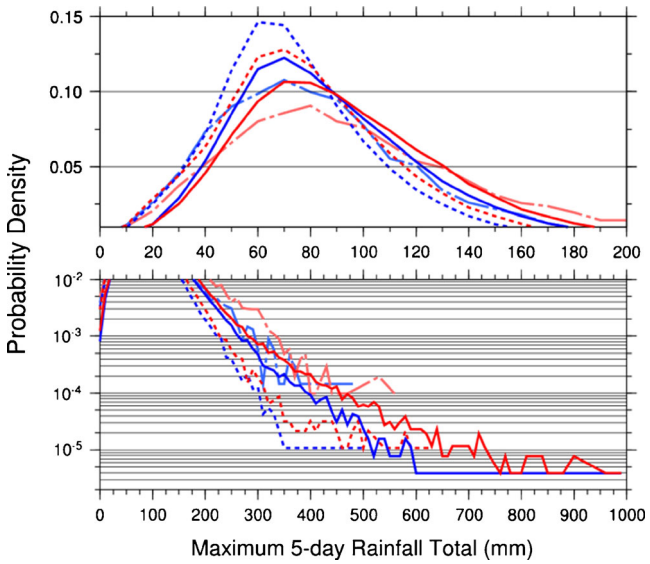

Fig. 11 PDF for RX5D (annual maximum 5-day rainfall total; millimeters) in the land areas. *Blue and red curves* indicate present-day and the future climates; *solid*, *dot*, and *dash-dot lines* are results from the 20-km-mesh, 60-km-mesh, and the 180-km-mesh models

highest for the 60-km-mesh model and lowest for the 180-km-mesh model. In contrast, within the RX5D range from 100 mm and especially from 200 to 500 mm, the PDFs for the 20-km- and 180-km-mesh models were similar for both the present and future climates. This complicated dependence on the horizontal resolutions stems from the reproducibility of the RX5Ds depicted in Fig. 3. Because of the small size of landmasses, the low horizontal resolution of the 180-km-mesh model makes it insensitive to landmasses to the south of 20°N; therefore, it produces very strong RX5Ds over landmasses as if they were the ocean. The rain shadow on the lee side of the landmass, apparent in Fig. 6, may also be a cause of differences between the different horizontal resolution models.

In the future, the frequencies of RX5Ds greater than threshold values of 300, 500, and 700 mm were all projected to increase over the land surface by greater than 200 % in the 20-km-mesh AGCM (Table 3), and the future/present-day ratio of the frequency of RX5Ds greater than 500 mm was 374 %. Although the future/present-day ratio of the frequencies of TC-induced RX5Ds (F_{tc}/P_{tc}) was estimated to be about 250 % on average for the three threshold values, increases in the frequencies of TC-induced RX5Ds contributed only secondarily to the future/present-day ratio of all RX5Ds (F_{tc}/F_a). About 66 and 100 % of the occurrences of RX5Ds greater than 500 and 700 mm, respectively, in the present-day climate were due to TC-induced precipitation (P_{tc}/P_a). Those percentages will decrease to 49 and 68 % (F_{tc}/F_a), respectively, in the future. Therefore, precipitation induced by phenomena other than TCs was projected to be primarily responsible for the increase in the frequency of large RX5Ds.

In risk management studies, the probability of risk is obtained by multiplying exposure to people by the frequency of extremes with potential for adverse and harmful effects to occur. Therefore, assessments of impacts are focused on peopled areas, and independent projections are therefore essential for land areas and combined land and ocean areas. The areal mean RX5D for combined land and ocean areas is larger than the RX5D for land areas only (Table 1). The increase in the areal mean RX5D in the future is a few percent larger for land areas only than for combined land and ocean areas. This relationship is also found in the increase in the frequencies of RX5Ds for all three threshold values (Table 3). The frequencies of simulated TC-induced RX5Ds contributed to the frequencies of RX5Ds to the same extent in the present-day (P_{tc}/P_a) and future (F_{tc}/F_a) for the land-and-ocean areas, in contrast to the decrease in the contribution of TC-induced RX5Ds for land areas only. This difference reflects the fact that the total area of land with a decrease of TC-induced precipitation is greater than the area of land with an increase (Fig. 8). The decrease of TC formation to the south of 22.5°N in the study area (Murakami and Wang 2010) contributed to the changes in TC-induced precipitation.

4.2.2 CDD

The areal mean CDD was projected to increase in the future for all three horizontal resolutions, but with very low statistical significance, as was the case for the areal mean RX5D (Table 1). The peak of the CDD PDFs occurred near 10 days and was highest for the 20-km-mesh model and lowest for the 180-km-mesh model (Fig. 12), whereas at CDDs greater than 100 days the PDF was highest for the 180-km-mesh model and lowest for the 20-km-mesh model. This dependency on the horizontal resolution is reasonable and consistent with previous studies (e.g., Cheng and Knutson 2008). The dependency in part reflects the fact that low-resolution models cannot represent small-scale, or meso-β, precipitation systems that break up dry spells. In the future climate, changes in the 500-hPa vertical pressure velocity over land areas fluctuate around zero during the dry season, November to March (Fig. 13), an indication that the CDD

Table 3 Frequency of RX5Ds greater than the indicated threshold values in the present-day and future climates for the 20-km-mesh AGCM

Threshold values of RX5D (mm)			Land			Land+ocean		
			300	500	700	300	500	700
Frequency (count/25 years)	Present	All (P_a)	771	47	9	31,758	5,289	1,494
		TC (P_{tc})	209	31	9	17,569	4,371	1,366
	Future	All (F_a)	1,605	176	31	43,793	8,513	2,939
		TC (F_{tc})	510	87	21	23,298	7,293	2,707
Ratio (%)		F_a/P_a	208	374	344	138	161	197
		P_{tc}/P_a	27	66	100	55	83	91
		F_{tc}/F_a	32	49	68	53	86	92
		F_{tc}/P_{tc}	244	281	233	133	167	198

P and *F* denote frequencies of the present-day and the future climates, whereas the subscripts *a* and *tc* denote all and TC-induced precipitation

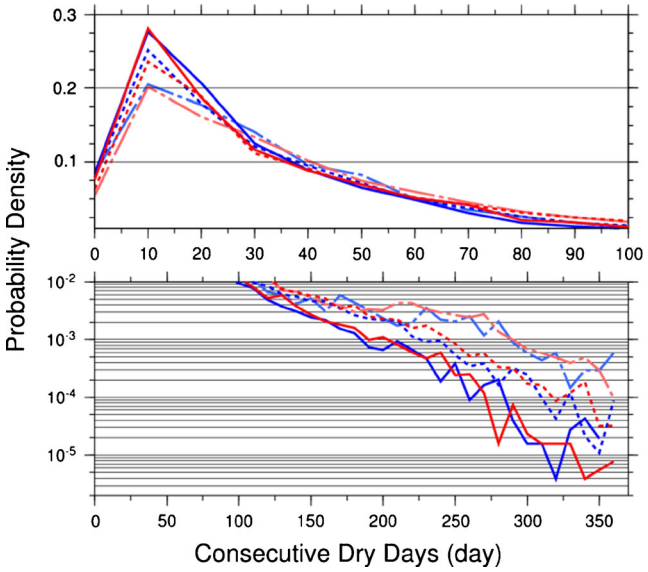

Fig. 12 Same as in Fig. 11 but for CDD (annual maximum consecutive dry days; day)

is determined by small-scale precipitation systems but not by large-scale circulation such as the Hadley cell. Intensification of Hadley cell circulation in the future, however, is responsible for the drying in these areas during the rainy season from May to October (e.g., Christensen et al. 2007).

The mean length of dry spells averaged over land areas with CDDs greater than 200 and 300 days per year is projected to decrease (Table 4), an indication that infrequent long CDDs greater than these threshold values will occur in the future over land areas with shorter mean dry spell lengths than is presently the case. The annual maximum dry spell length, like the annual number of consecutive dry days, changed in ways different from the mean dry spell length. In addition, the mean wet spell length over land areas was also projected to remain the same or decrease above threshold values of 200 and 300 wet days per year.

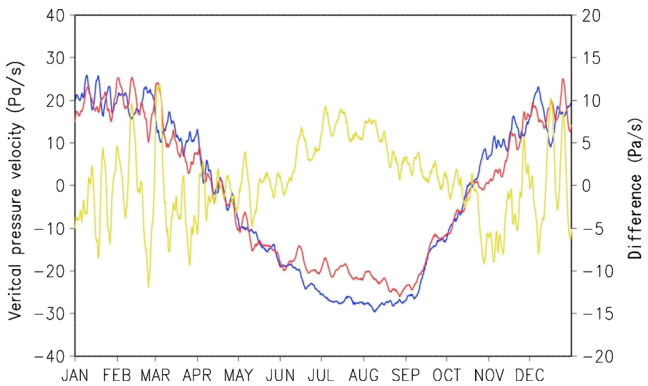

Fig. 13 Climatological 5-day running means of 500-hPa vertical velocity (Pascal per second) over the land areas. *Blue and red curves* indicate present-day and the future climates; *green* indicates the differences between the present-day and the future climates

The results presented in Table 4 reveal that infrequent long CDDs in the future can occur where both of the mean spell lengths decrease.

The mechanism responsible for prolonged drought over Mexico and Central America in the present-day climate is not well understood because easterly waves, which are a source of precipitation, may (Serra et al. 2010) or may not (Méndez and Magaña 2010) be enhanced by the CLLJ over the Caribbean Sea. Better understanding of such mechanisms that are responsible for CDDs should help improve climate projections and impact studies.

5 Discussion

5.1 Horizontal resolution

Kitoh et al. (2011), using the same experimental setup as the present study, noted that the 20-km-mesh model projected larger increases in RX5D in South America than the 60-km-mesh model ensemble. They concluded that the difference resulted from the resolution dependency of extreme precipitation totals and the difficulty in quantifying precipitation changes at local levels. In our results (Fig. 5), the same effect of resolution on projected RX5Ds is apparent as well, but such a dependency is less obvious in the comparison of the 20-km- and 60-km-mesh model CDDs in Fig. 6. One possible reason is that RX5D is associated with small-scale heavy precipitation, whereas CDD is associated with large-scale persistent dry conditions. Hall et al. (2012)) concluded that there were no significant changes in CDDs in the Caribbean, a conclusion that is consistent with Table 1. We found significant changes there (Fig. 5a), although the changes are not consistent among all members of the 60-km-mesh model ensemble.

The future increase in the areal mean CDD is about 9 % for land areas as well as for land-and-ocean areas and is unaffected by the horizontal resolution of the models (Table 1). The horizontal resolution dependency is the same for the land-and-ocean areas and the land areas only. As mentioned above, this is not the case for the RX5D (Table 1). These dependencies of RX5Ds and CDDs on horizontal resolution suggest that we should be cautious in the qualitative and quantitative use of extreme indices projected with low-horizontal-resolution models because the dependencies on resolution are different from one index to another. In addition, changes in mean dry spell lengths for the land areas are opposite in sign to those of the land and ocean areas (Table 4). This fact underscores the importance of a clear land-ocean separation, which requires high horizontal resolution of GCMs and RCMs.

Projected changes in TC occurrence are controversial; both an increase (Vecchi and Soden 2007; Sugi et al.

Table 4 Mean dry and wet spell lengths averaged over areas with CDD greater than the indicated threshold values for present-day and future climates in the 20-km-mesh AGCM

Threshold values of CDD (day)		Land			Land+ocean		
		100	200	300	100	200	300
Mean dry spell lengths (day)	Present	23.6	49.0	113.0	24.6	51.5	93.4
	Future	24.4	46.4	102.0	23.2	48.9	105.0
Mean wet spell lengths (day)	Present	2.81	1.64	1.55	2.71	1.70	1.57
	Future	3.29	1.66	1.19	3.00	1.90	1.29

2009) and a decrease (Knutson et al. 2008; Zhao et al. 2009) have been proposed because the change appears to be sensitive to changes in the spatial pattern of SSTs (Murakami and Wang 2010). Further projections with high-horizontal-resolution models that can resolve basic TC structures may be essential for consistent projections of changes in TC-induced RX5Ds.

Although we did not discuss the projected results with the 180-km-mesh model ensemble, the large-scale geographical patterns obtained are similar to the patterns obtained with the 60-km-mesh model, but the results differ quantitatively. The spatial contrasts of changes in CDDs, and especially RX5Ds, are diluted because of the low horizontal resolution of the 180-km-mesh model.

5.2 Methodology

We used the same detrended observed SST interannual variations for both present-day and future climate simulations, and this fact may have affected the projected changes. However, Aguilar et al. (2005) showed no correlation between eastern Pacific SSTs and precipitation extremes based on observations in Central America and the Caribbean. In addition, low-frequency modulators, such as the Atlantic multidecadal oscillation and Pacific decadal oscillation, may contribute secondarily to the spatial pattern of prolonged droughts in Mexico and Central America (Méndez and Magaña 2010). We did not include these decadal phenomena in our experimental design because of their very high uncertainties. Additional uncertainty in the changes in the two precipitation-related indices should therefore be kept in mind.

The prescribed lower boundary conditions have 1° of horizontal resolution and 1-month temporal resolution because we employed the monthly mean 1° observed SST and sea-ice concentration. Fine-scale spatial or temporal SST variability may drive extremes and TCs. However, we were unable to project such variability because of the chaotic nature of the atmosphere and ocean.

There is ambiguity in partitioning precipitation into TC-induced and non-TC fractions because some TCs accompany a front or other precipitation system. The contributions of the annual TC-induced precipitation to the annual total precipitation in previous observational studies have been 3–4 % for a 444-km radius (Rodgers et al. 2001) and 8–9 % for a 500-km radius (Jiang and Zipser 2010). We varied the radius of the TC-induced precipitation, but the ratios in Table 3 are consistent, although the frequencies become smaller as the radius becomes smaller. This is partly because the extent of TC-induced precipitation in the model is smaller than the scale of the observations.

5.3 Biases

All the models have biases in both the climatological mean states and the extreme phenomena in the present-day climate simulations. In impact assessments, adaptation designs, risk managements, statistical bias corrections are widely applied using mean ratios, PDF, or other bias techniques as practical and second best (e.g., Bao et al. 2010; Watanabe et al. 2012). From the climatological point of view, it is interesting to know how the biases affect the projections but has rarely been explored. We need to explore at least two points even if we simplified the issues under the additivity: how the biases in the climatological mean states affect the extreme phenomena in the present-day climate and affect the mean states in the future climate. This issue should be addressed to raise the reliability of the future climate projections.

6 Concluding summary

We used 20-km-, 60-km-, and 180-km-mesh atmospheric global general circulation models to explore projected changes in RX5Ds and CDDs, and we used an ensemble approach to quantify the uncertainty of the changes. The annual maximum 5-day rainfall total, RX5D, was projected to increase in the future (2075–2099) throughout almost all of the study area. Changes in RX5D that were not statistically significant were found in central Mexico, western Nicaragua, and several other small areas. The annual maximum number of consecutive dry days, CDD, was projected to significantly increase in Central America and the Caribbean, except in eastern Mexico and other small areas. Large changes in CDD were apparent in western Mexico, Nicaragua, and western Panama.

The dependency of the RX5D PDFs on the horizontal resolution of the models was quite complicated, although the increases in RX5D were consistent among the three different horizontal resolution AGCMs. This fact suggests that one should be wary of artifacts caused by the dependency of the RX5Ds on horizontal resolution. In contrast, the dependency of the CDD PDFs on horizontal resolution was simple. All three different horizontal resolution AGCMs projected that infrequent large extremes of both RX5D and CDD would become more common. In addition, precipitation unrelated to tropical cyclone phenomena was primarily responsible for the increase in frequency of extreme RX5Ds.

The present study revealed that future climate projections with a high horizontal resolution model are essential for small landmass areas such as the study area because the distributions of land, ocean, and orography, and phenomena such as TCs and rain shadow effects distinctly influence changes in precipitation-related indices in models of future climates.

Our time-slice experimental approach does not take into account atmosphere–ocean interactions and hence may overestimate the intensity and lifetime of TCs because ocean–atmosphere interactions induce upwelling, reduce SSTs, and therefore inhibit the development of TCs. These effects are apparent in the present-day climate. We are planning to perform AGCM experiments with a slab-ocean or full-ocean model to overcome this drawback.

Infrequent but high-impact extremes are difficult to reproduce and are projected in state-of-the-art AGCMs. The PDF for such extremes is essential for risk management. We need better simulations and projections, and we need to identify how best to exploit current simulations.

Acknowledgments This work was funded by the "Development of Infrastructural Technology for Risk Information on Climate Change" of the Ministry of Education, Culture, Sports, Science and Technology of Japan (MEXT). The Earth Simulator of the Japan Agency for Marine-Earth Science and Technology (JAMSTEC) made it possible to perform the very large calculations.

References

Adler RF, Huffman GJ, Bolvin DT, Curtis S, Nelkin EJ (2000) Tropical rainfall distributions determined using TRMM combined with other satellite and rain gauge information. J Appl Meteorol l39:2007–2023. doi:10.1175/1520-0450(2001)040<2007:TRDDUT>2.0.CO;2

Aguilar E et al (2005) Changes in precipitation and temperature extremes in Central America and northern South America. 1961–2003. J Geophys Res 110, D23107

Arritt RW, Rummukainen M (2011) Challenges in regional-scale climate modeling. Bull Amer Meteor Soc 92:365–368. doi:10.1175/2010BAMS2971.1

Bao L, Gneiting T, Grimit EP, Guttorp P, Raftery AE (2010) Bias correction and Bayesian model averaging for ensemble forecasts of surface wind direction. Mon Weather Rev 138:1811–1821. doi:10.1175/2009MWR3138.1

Bengtsson L, Botzet M, Esch M (1996) Will greenhouse gas induced warming over the next 50 years lead to higher frequency and greater intensity of hurricanes? Tellus 48A:57–73

Campbell JD, Taylor MA, Stephenson TS, Watson RA, Whyte FS (2011) Future climate of the Caribbean from a regional climate model. Int J Climatol 31:1866–1878. doi:10.1002/joc.2200

Cheng C-T, Knutson T (2008) On the verification and comparison of extreme rainfall indices from climate models. J Climate 21:1605–1621. doi:10.1175/2007JCLI1494.1

Christensen JH et al (2007) Regional climate projections. In: Solomon SD (ed) Climate change 2007: the physical science basis. Contribution of Working Group I to the Fourth Assessment Report of the Intergovernmental Panel on Climate Change. Cambridge University Press, Cambridge, pp 847–940

Fábrega J, Nakaegawa T, Pinzón R, Nakayama R, Arakawa O, SOUSEI Theme-CModeling group (2013) Hydroclimate projections for Panama in the late 21st century. Hydroll Res Lett 7:23–29. doi:10.3178/hrl.7.23

Frich P, Alexander L, Della-Marta P, Gleason B, Haylock M, Tank AK, Peterson T (2002) Observed coherent changes in climate extremes during the second half of the twentieth century. Clim Res 19:193–212. doi:10.3354/cr019193

Giorgi F (2006) Climate change hot-spots. Geophys Res Lett 33, L08707. doi:10.1029/2006GL025734

Hall TC, Sealy AM, Stephenson TS, Taylor MA, Chen AA (2012) Future climate of the Caribbean from a super-high resolution atmospheric general circulation model. Theor Appl Climatol. doi:10.1007/s00704-012-0779-7

Huffman GJ, Adler RF, Morrissey MM, Bolvin DT, Curtis S, Joyce R, McGavock B, Susskind J (2001) Global precipitation at one-degree daily resolution from multi-satellite observations. J Hydrometeorol 2:36–50. doi:10.1175/1525-7541(2001)002<0036:GPAODD>2.0.CO;2

Jiang H, Zipser EJ (2010) Contribution of tropical cyclones to the global precipitation from 8 seasons of TRMM data: regional, seasonal, and interannual variations. J Climate 23:1526–1543. doi:10.1175/2009JCLI3303.1

Jung T, Miller MJ, Palmer TN, Towers P, Wedi N, Achuthavarier D, Adams JM, Altshuler EL, Cash BA, Kinter JL III, Marx L, Stan C, Hodges KI (2012) High-resolution global climate simulations with the ECMWF model in Project Athena: experimental design, model climate, and seasonal forecast skill. J Climate 25:3155–3172. doi:10.1175/JCLI-D-11-00265.1

Kamiguchi K, Kitoh A, Uchiyama T, Mizuta R, Noda A (2006) Changes in precipitation-based extremes indices due to global warming projected by a global 20-km-mesh atmospheric model. SOLA 2:64–67. doi:10.2151/sola.2006-017

Karmalkar AV, Bradley RS, Diaz HF (2008) Climate change scenario for Costa Rican montane forests. Geophys Res Lett 35, L11702. doi:10.1029/2008GL033940

Karmalkar AV, Bradley RS, Diaz HF (2011) Climate change in Central America and Mexico: regional climate model validation and climate change projections. Climate Dynam 37:605–629. doi:10.1007/s00382-011, 1099–9

Kitoh A, Ose T, Kurihara K, Kusunoki S, Sugi M, KAKUSHIN Team-3 Modeling Group (2009) Projection of changes in future weather extremes using super-high-resolution global and regional atmospheric models in the KAKUSHIN Program: results of preliminary experiments. Hydrol Res Lett 3:49–53. doi:10.3178/hrl.3.49

Kitoh A, Kusunoki S, Nakaegawa T (2011) Climate change projections over South America in the late twenty-first century with the 20-km and 60-km mesh MRI-AGCM. J Geophys Res 116, D06105. doi:10.1029/2010JD014920

Knaff JA (1997) Implications of summertime sea level pressure anomalies in the tropical Atlantic region. J Climate 10:789–804

Knutson TR, Sureties JJ, Garner ST, Vecchi GA, Held IM (2008) Simulated reduction in Atlantic hurricane frequency under twenty-first-century warming conditions. Nat Geosci 1:359–364. doi:10.1038/ngeo202

Méndez M, Magaña V (2010) Regional aspects of prolonged meteorological droughts over Mexico and Central America. J Climate 23:1175–1188. doi:10.1175/2009JCLI3080.1

Min S-K, Zhang X, Zwiers FW, Hegerl GC (2011) Human contribution to more-intense precipitation extremes. Nature 470:378–381. doi:10.1038/nature09763

Mizuta R, Oouchi K, Yoshimura H, Noda A, Katayama K, Yukimoto S, Hosaka M, Kusunoki S, Kawai H, Nakagawa M (2006) 20-km-mesh global climate simulations using JMA-GSM model—mean climate states—. J Meteor Soc Japan 84:165–185

Mizuta R, Adachi Y, Yukimoto S, Kusunoki S (2008) Estimation of the future distribution of sea surface temperature and sea ice using the CMIP3 multi-model ensemble mean. Technical Report of the Meteorological Research Institute 56: 28

Murakami H, Sugi M (2010) Effect of model resolution on tropical cyclone climate projections. SOLA 6:73–76. doi:10.2151/sola.2010-019

Murakami H, Wang B (2010) Future change of North Atlantic tropical cyclone tracks: projection by a 20-km-mesh global atmospheric model. J Climate 23:2699–2721. doi:10.1175/2010JCLI3338.1

Nakaegawa T, Kitoh A, Hosaka M (2013a) Discharge of major global rivers in the late 21st century climate projected with the high horizontal resolution MRI-AGCMs—overview—. Hydrol Process 27. doi:10.1002/hyp.9831

Nakaegawa T, Kitoh A, Ishizaki Y, Kusunoki S, Murakami H (2013b) Caribbean low-level jets and accompanying moisture fluxes in a global warming climate projected with CMIP3 multi-model ensemble and fine-mesh atmospheric general circulation models. Int J Climatol 33. doi:10.1002/joc.3733

Neelin JD, Münnich M, Su H, Meyerson JE, Holloway CE (2006) Tropical drying trends in global warming models and observations. Proc Nat Acad Sci 103:6110–6115. doi:10.1073/pnas.0601798103

Rauscher SA, Giorgi F, Diffenbaugh NS, Seth A (2008) Extension and intensification the Meso-American mid-summer drought in the twenty-first century. Climate Dyn 31:551–571. doi:10.1007/s00382-007-0359-1

Rayner NA, Parker DE, Horton EB, Folland CK, Alexander LV, Rowell DP, Kent EC, Kaplan A (2003) Global analyses of sea surface temperature, sea ice, and night marine air temperature since the late nineteenth century. J Geophys Res 108:4407. doi:10.1029/2002JD002670

Rodgers EB, Adler RF, Pierce HF (2001) Contribution of tropical cyclones to the North Atlantic climatological rainfall as observed from satellites. J Appl Meteor 40:1785–1800. doi:10.1175/1520-0450(2001)040<1785:COTCTT>2.0.CO;2

Senevirante SI et al (2012) Changes in climate extremes and their impacts on the natural physical environment. In: Field CB (ed) Managing the risks of extreme events and disasters to advance climate change adaptation. Cambridge University Press, Cambridge, pp 109–230

Serra YL, Kiladis GN, Hodges KI (2010) Tracking and mean structure of easterly waves over the Intra-Americas Sea. J Climate 23:4823–4840. doi:10.1175/2010JCLI3223.1

Sugi M, Murakami H, Yoshimura J (2009) A reduction in global tropical cyclone frequency due to global warming. SOLA 5:164–167. doi:10.2151/sola.2009-042

Takaya Y, Yasuda T, Ose T, Nakaegawa T (2010) Predictability of the mean location of typhoon formation in a seasonal prediction experiment with a coupled general circulation model. J Meteor Soc Japan 88:799–812. doi:10.2151/jmsj.2010-502

Taylor MA, Whyte FS, Stephenson TS, Campbell JD (2012) Why dry? Investigating the future evolution of the Caribbean Low Level Jet to explain projected Caribbean drying. Int J Climatol 32:119–128. doi:10.1002/joc.3461

Tebaldi C, Hayhoe K, Arblaster JM, Meehl GA (2006) Going to the extremes: an intercomparison of model-simulated historical and future changes in extreme events. Clim Change 79:185–211. doi:10.1007/s10584-006-9051-4

Uchiyama T, Mizuta R, Kamiguchi K, Kitoh A, Noda A (2006) Changes in temperature-based extremes indices due to global warming projected by a global 20-km-mesh atmospheric model. SOLA 2:68–71. doi:10.2151/sola.2006-018

van der Linden P, Mitchell JFB (2009) ENSEMBLES: climate change and its impacts: summary of research and results from the ENSEMBLES project. Met Office Hadley Centre, Exeter, p 160

Vecchi GA, Soden BJ (2007) Global warming and the weakening of the tropical circulation. J Climate 20:4316–4340. doi:10.1175/JCLI4258.1

Vitart FD, Stockdale TN (2001) Seasonal forecasting of tropical storms using coupled GCM integrations. Mon Wea Rev 129:2521–2537. doi:10.1175/1520-0493(2001)129<2521:SFOTSU>2.0.CO;2

Walsh K, Fiorino M, Landsea C, McInnes K (2007) Objectively-determined resolution-dependent threshold criteria for detection of tropical cyclones in climate models and reanalyses. J Climate 20:2307–2314. doi:10.1175/JCLI4074.1

Watanabe S, Kanae S, Seto S, Yeh PJF, Hirabayashi Y, Oki T (2012) Intercomparison of bias-correction methods for monthly temperature and precipitation simulated by multiple climate models. J Geophys Res 117, D23114. doi:10.1029/2012JD018192

Zhao M, Held IM, Lin S-J, Vecchi GA (2009) Simulations of global hurricane climatology, interannual variability, and response to global warming using a 50-km resolution GCM. J Climate 22:6653–6678. doi:10.1175/2009JCLI3049.1